Chapter 8

Conclusions and Implications for Interstellar Chemistry

The studies presented in this thesis involve the rotational spectroscopic characterization of and observational searches for several key prebiotic molecules. A summary of the results of these studies and a discussion of their implications and future applications are presented below.

8.1 Laboratory Rotational Spectroscopy

Combined studies using the original Fourier Transform Microwave Spectrometer and the Caltech and JPL Direct Absorption Flow Dell Spectrometers were conducted to obtain the microwave, millimeter, and submillimeter spectra of several key prebiotic species. The CALPGM program suite and the SMAP spectral analysis program were then used to assign these data and determine the spectroscopic parameters for each species.

The ground and first four vibrational states of the 3C ketose, dihydroxyacetone, are now characterized up to 450 GHz. The spectral analysis of its 3C structural isomer, dimethyl carbonate, was quite limited because of the weak nature of the spectrum, but the K_a=0, 1 lines of this species have been assigned up to 360 GHz. In the case of another 3C structural

isomer, methyl glycolate, full characterization of the ground state up to 360 GHz has been completed. The analyses of dimethyl carbonate and methyl glycolate present challenges to current internal rotation models. Additional higher sensitivity laboratory investigation of dimethyl carbonate is required, and the results of such a study might enable a more complete model to be developed. In addition, assignments of the pure rotational lines in the many torsional states of methyl glycolate should be completed.

The pure rotational analysis of the ground and first three vibrational states of the 2C α-hydroxy aldehyde, glycolaldehyde, has also been completed for frequencies up to 354 GHz. A similar analysis to 305 GHz has been completed for the second most complex aminoalcohol, aminoethanol, which is a predicted interstellar grain surface product and the suspected precursor to the amino acid alanine.

The information gained in these studies was used to guide subsequent observational searches, the results of which are discussed in the next section. The vibrational state analyses also provided the necessary information to determine accurate partition functions for these molecules. It is clear from the dihydroxyacetone and glycolaldehyde studies that the vibrational state contribution to the partition functions of such complex molecules is significant, and these results will influence future such calculations in observational astronomy.

The results of the microwave/millimeter-wave studies will be used as a starting point for further characterization of these types of molecules in the THz spectral range as appropriate laboratory techniques are developed. THz laboratory work will provide the necessary information to guide searches with the CASIMIR instrument on the SOFIA observatory and the HIFI instrument on the Herschel Observatory. Species such as those studied here often have much stronger torsional bands than rotational bands, and so observational searches

for molecules such as dimethyl carbonate may indeed become possible with these new high frequency instruments if the appropriate spectral information is available.

8.2 Observational Astronomy

The results of the laboratory studies were used to guide observational searches for these species with the CSO, OVRO, and GBT observatories. Glycolaldehyde was previously detected in the Sgr B2(N-LMH) hot core, and so no searches for this species were conducted.

The key result of the CSO searches in particular is the first observational evidence for an interstellar ketose, dihydroxyacetone, which was detected at a higher column density than any other similarly complex species previously observed in the Sgr B2(N-LMH) hot core. The rotational temperature and line center velocities imply that this emission arises from the hot core rather than from the cooler extended envelope. Attempts at imaging this emission were unsuccessful, but more sensitive studies will be conducted after commissioning of the CARMA observatory. The sensitivity level required for confirming GBT observations of low-energy transitions was not reached. The nine lines observed with the CSO make a strong case for the presence of this species, but these results must be confirmed before a definitive detection can be claimed.

The more stable 3C structural isomers are expected to be formed by any process leading to dihydroxyacetone. Searches are planned for dimethyl carbonate and methyl glycolate, but no observations have been completed at this time. Lines that could be attributed to methyl glycolate were observed in a 3 mm survey of the Sgr B2(N-LMH) source, however, and a preliminary analysis places this species at an even higher column density than that determined for dihydroxyacetone. The CSO/BIMA results and earlier studies of 2C compounds make it clear that structural isomerism plays an important role in interstellar

chemistry.

Aminoethanol was not detected in any hot core source, and the limits derived for its column density call into question the proposed grain surface pathways leading to its formation. If aminoalcohols are not produced by single-atom addition reactions on grain surfaces, then new interstellar formation pathways for amino acids may be required.

The combined results of the laboratory and observational studies indicate that prebiotic chemistry does indeed achieve high levels of complexity well before incorporation into a parent body. These results raise serious questions about the validity of current interstellar chemical models and imply that complex interstellar chemistry is very poorly understood. The extremely large abundances of the 3C species relative to much simpler species coupled with the lack of observational evidence for one of the simplest predicted grain surface species indicates that current interstellar chemistry models require extensive revision. Chemical pathways that may explain these results do exist, but have not yet been considered for complex interstellar chemistry. These pathways are compared to existing chemical models below, and their implications in light of the conclusions drawn from the work presented here are discussed.

8.3 Implications for Interstellar Chemistry

Early interstellar chemical models considered complex molecule formation on grains [12], but current models for interstellar chemistry rely on both solid and gas phase reactions for the formation of the most complex interstellar organic molecules, which tend to be the simplest examples of various compounds (alcohols, ethers, esters, etc.). There are two main grain surface chemistry mechanisms used in these models, namely radical-radical reactions and single-atom addition reactions. Both classes of models rely on initial single-

atom addition reactions to form simple radicals. The subsequent processing of these radicals is treated quite differently, however, in these two classes of models.

In the first approach, the radicals formed from single-atom addition reactions undergo radical-radical combination to form more complex species (see [69–72]). Many of these higher order reactions are those included in the model by Allen and Robinson [12], but only a subset of the complex reactions included in this earlier work are considered in more recent models. These models assume that these species are in constant flux with the gas phase, where they can undergo ion-molecule reactions to form even more complex species. The most recent of these models has also considered photolysis effects on the grain surface chemistry [72], though very little information is provided as to the molecules undergoing photolysis or the branching ratios for the photolysis pathways. Likewise, some of the reactions involving major photolysis products that are included in the earlier grain surface model [12] are not considered in this work.

The second approach for grain surface chemical models involves only single-atom addition reactions. Gas phase reactions in interstellar clouds can efficiently form CO, N_2, O_2, C_2H_2, and C_2H_4, and these species are thought to accrete onto grain surfaces and undergo single-atom addition reactions [3, 73, 74]. Four basic principles developed from the conditions and limitations of grain surface chemistry guide this class of models. Due to the overwhelming abundance of hydrogen in the interstellar medium, it is assumed that the great majority of grain chemistry is driven by the reaction of hydrogen atoms with multiply-bonded molecules and surface radicals. It is also assumed that multiple bonds in any single molecule are broken in order of hydrogen-tunnelling energy barriers, beginning with the lowest barrier. Radical stability is imposed on all intermediates predicted by these reactions, eliminating all reactions with unstable intermediates from appearing in

the model. Also, pathways involving migration or reaction between two radicals are not permitted. Many potential grain surface reaction pathways are eliminated by the conditions imposed, greatly simplifying the possible products of grain synthesis. The simplest case for such a reaction network, as is shown in Figure 8.1, predicts that such a system will not extend in molecular complexity beyond alcohols and aminoalcohols without subsequent gas phase ion-molecule reactions.

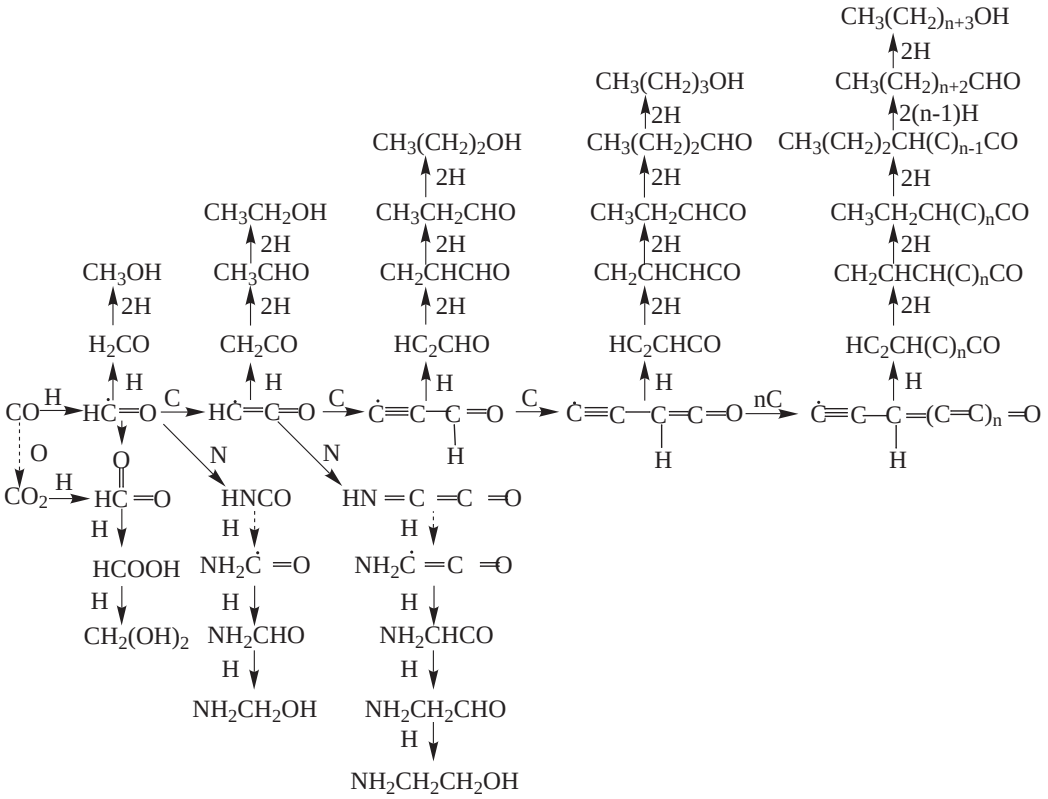

Figure 8.1: The simplest chemical model of grain surface reactions driven by single-atom addition to CO [3].

Both classes of models predict the formation of more complex species by gas phase ion-molecule reactions. It has been shown, however, that such processes are insufficient for the production of such complex organic species as ethanol (CH_3CH_2OH) and methyl formate (CH_3OCHO) [13]. Organics such as acetaldehyde (CH_3CHO), ethanol, methyl formate,

acetic acid (CH_3COOH), and glycolaldehyde (CH_2OHCHO) have also been detected in high abundance in regions of grain mantle disruption and evaporation, suggesting that these species are formed on grain surfaces [15, 18, 19, 75]. The mechanisms for complex molecule production on grains are clearly much more important, and much more complex, than has been recognized.

Recent observational studies, including those presented in Chapters 4 and 5, have offered insight into the mechanisms for grain surface synthesis. The relative hot core abundances of the 2C structural isomers methyl formate, acetic acid, and glycolaldehyde (52:2:1, respectively [16]) indicate that if they form on grains it is not from kinetically-controlled single-atom addition reactions. Likewise, the 3C aldose sugar, glyceraldehyde ($CH_2OHCHOHCHO$), was not detected in Sgr B2(N-LMH) [76] while the 3C ketose sugar, dihydroxyacetone ($CO(CH_2OH)_2$), was detected in this source (see Chapter 4). Another 3C structural isomer, methyl glycolate ($HOCH_2COOCH_3$), has also been tentatively detected in the Sgr B2(N-LMH) source at twice the abundance of dihydroxyacetone (see Chapter 5). These observed abundances follow the pattern of the relative thermodynamic stability (see Appendix D), with the more stable structural isomers being more abundant. The notable exception to this trend is acetic acid, which is much less abundant than methyl formate but is the most thermodynamically stable of the 2C isomers. Acids undergo esterification reactions in the presence of alcohols, which comprise a large fraction of ice grain surface material. Relative reactivity should therefore also be considered, as the observed abundance of any highly reactive species should be lower than predicted by any simple reaction network.

These results require that new chemical processes be incorporated into existing grain surface chemical models, and the first step toward more accurate models is to consider complex molecule formation. Reactions of the type originally proposed by Allen and

Robinson [12] can lead to the complex organics being sought, but expansion of this original network is required to explain the 3C compounds. Ice grain mantles in dense clouds are known to be comprised primarily of H_2O, CH_3OH, CO, and NH_3, and varying ratios of these species are used in laboratory studies of grain surface chemistry [10]. All of the 2C and 3C species, as well as many others observed in hot cores, can be formed from reactions involving these species and their radical precursors through addition of radicals to carbonyl functional groups. These types of reactions have not been considered in previous grain surface models. *Ab initio* studies have shown that the barriers to radical abstraction of an aldehyde proton are much lower than the barriers to radical addition to the aldehyde group [77]. The aldehyde radicals produced by these abstractions could then undergo further radical-radical combination reactions with other more mobile surface species. It is possible that these types of abstraction and aldehyde radical reactions could lead to a wide array of organics on grain surfaces. A chemical network involving these reactions and its implications for grain surface chemistry are outlined below.

8.3.1 Proposed Grain Surface Chemical Network

The chemical network presented here is based on the photolysis products of the major grain mantle species H_2O, CH_3OH, CO, and NH_3. The photolysis pathways and rates for these species in dense clouds are presented in Table 8.1 [78] and [79]. The photolysis rates for each pathway are determined by the product of the branching ratio and this overall rate. Water photolysis is dominated by the OH pathway, which has branching ratios ranging from 0.9 to 0.99 [80]. Investigation of methanol photolysis branching ratios has only been conducted at a few wavelengths, and only gas phase experiments were conducted in the most quantitative study [81]. The branching ratio for the CH_3O pathway was determined

to be 0.86, but it is not clear if this is applicable for the solid state. *Ab initio* studies indicate that the CH_2OH pathway is the most energetically favored, and so it is possible that it is the secondary photolysis product, but there are no laboratory results to support this hypothesis [82]. Clearly these branching ratios will drastically affect the grain surface chemistry, and laboratory experiments should be conducted to examine methanol photolysis in ices.

Table 8.1: Photolysis pathways and rates for major grain mantle components in dense interstellar clouds at A_v=6.

							Γ_{total} (s^{-1})
NH_3	+	hν	→	NH_2	+	H	3.43×10^{-15}
CH_3OH	+	hν	→	CH_3	+	OH	3.09×10^{-15}
			→	CH_3O	+	H	
			→	CH_2OH	+	H	
H_2O	+	hν	→	H	+	OH	1.22×10^{-14}
			→	O	+	H_2	
CO	+	hν	→	C	+	O	7.61×10^{-20}

While most of the photolysis products listed in Table 8.1 have been included in previous models, reactions involving CH_3O have not been considered in any but the original model by Allen and Robinson [12], and in this case only the simplest reactions were considered. Many higher order reactions involving CH_2OH were also excluded from this and subsequent models. These radicals will play critical roles in grain surface chemistry if they are indeed the primary methanol photolysis products.

Dense clouds are typically at 10 K, and the photolysis products listed in Table 8.1 are mobile on grain surfaces at this temperature. Periodic warm-up events to as high as 50 K are also possible, especially in star forming regions, and the heavier species will become much more mobile at these temperatures. CO reactions are important on grain surfaces,

and these are outlined in Table 8.2. The mobile radical species can also form more complex species through activationless radical-radical reactions such as those outlined in Table 8.3. Aldehydes formed by these reactions could then undergo proton abstraction reactions such as those summarized in Table 8.4. The resultant radicals would not be very mobile on grain surfaces, but the more mobile photolysis products could certainly recombine with these species to produce highly complex products through the reactions shown in Table 8.5. The rate constants for these reactions have been determined by the method outlined in the next section.

Table 8.2: Reactions of CO with surface radicals.

							E_a	k (cm^3/s)	
							(K)	10 K	50 K
OH	+	CO	→	CO_2	+	H	300	1.07×10^{-12}	$6.33\times10^{+00}$
H	+	CO	→	HCO			1000	$6.03\times10^{+06}$	$4.30\times10^{+07}$
O	+	CO	→	CO_2			0	$1.58\times10^{+03}$	$3.75\times10^{+11}$

Table 8.3: Radical-radical reactions between photolysis products and secondary radicals.

					k (cm^3/s)	
					10 K	50 K
H	+	H	→	H_2	$3.83\times10^{+12}$	$2.73\times10^{+13}$
H	+	NH_2	→	NH_3	$1.92\times10^{+12}$	$1.39\times10^{+13}$
H	+	CH_3	→	CH_4	$1.92\times10^{+12}$	$1.37\times10^{+13}$
H	+	OH	→	H_2O	$1.92\times10^{+12}$	$1.37\times10^{+13}$
H	+	CH_3O	→	CH_3OH	$1.92\times10^{+12}$	$1.36\times10^{+13}$
H	+	CH_2OH	→	CH_3OH	$1.92\times10^{+12}$	$1.36\times10^{+13}$
H	+	O	→	OH	$1.92\times10^{+12}$	$1.40\times10^{+13}$
C	+	O	→	CO	$3.41\times10^{+03}$	$7.48\times10^{+11}$
H	+	C	→	CH	$1.92\times10^{+12}$	$1.40\times10^{+13}$
NH_2	+	NH_2	→	NH_2NH_2	$6.24\times10^{+02}$	$5.15\times10^{+11}$
NH_2	+	CH_3	→	NH_2CH_3	$3.12\times10^{+02}$	$3.08\times10^{+11}$
NH_2	+	OH	→	NH_2OH	$3.12\times10^{+02}$	$3.08\times10^{+11}$
NH_2	+	CH_3O	→	NH_2OCH_3	$3.12\times10^{+02}$	$2.59\times10^{+11}$
NH_2	+	CH_2OH	→	NH_2CH_2OH	$3.12\times10^{+02}$	$2.58\times10^{+11}$
CH_3	+	CH_3	→	CH_3CH_3	8.73×10^{-02}	$1.01\times10^{+11}$
CH_3	+	OH	→	CH_3OH	4.57×10^{-02}	$7.76\times10^{+10}$
CH_3	+	CH_3O	→	CH_3OCH_3	4.36×10^{-02}	$5.21\times10^{+10}$
CH_3	+	CH_2OH	→	CH_3CH_2OH	4.36×10^{-02}	$5.07\times10^{+10}$
OH	+	OH	→	HOOH	4.18×10^{-03}	$5.42\times10^{+10}$
OH	+	CH_3O	→	$HOOCH_3$	2.09×10^{-03}	$2.86\times10^{+10}$
OH	+	CH_2OH	→	$HOCH_2OH$	2.09×10^{-03}	$2.72\times10^{+10}$
CH_3O	+	CH_3O	→	CH_3OOCH_3	4.53×10^{-09}	$3.09\times10^{+09}$
CH_3O	+	CH_2OH	→	CH_3OCH_2OH	2.27×10^{-09}	$1.66\times10^{+09}$
CH_2OH	+	CH_2OH	→	$HOCH_2CH_2OH$	6.41×10^{-15}	$2.29\times10^{+08}$
H	+	HCO	→	H_2CO	$1.92\times10^{+12}$	$1.36\times10^{+13}$
NH_2	+	HCO	→	NH_2CHO	$5.14\times10^{+05}$	$1.02\times10^{+12}$
CH_3	+	HCO	→	H_3CCHO	4.36×10^{-02}	$5.56\times10^{+10}$
OH	+	HCO	→	HOCHO	2.09×10^{-03}	$3.21\times10^{+10}$
CH_3O	+	HCO	→	CH_3OCHO	9.26×10^{-07}	$6.56\times10^{+09}$
CH_2OH	+	HCO	→	$HOCH_2CHO$	9.23×10^{-07}	$5.13\times10^{+09}$
HCO	+	HCO	→	OHCCHO	1.85×10^{-06}	$1.00\times10^{+10}$
CH	+	H	→	CH_2	$1.92\times10^{+12}$	$1.45\times10^{+13}$
CH_2	+	H	→	CH_3	$1.92\times10^{+12}$	$1.38\times10^{+13}$

Table 8.4: Aldehyde proton abstraction reactions.

							k (cm^3/s)	
							10 K	50 K
H	+	HCOOH	→	H_2	+	COOH	7.20×10^{-01}	$5.12\times10^{+00}$
NH_2	+	HCOOH	→	NH_3	+	COOH	2.30×10^{-41}	1.90×10^{-32}
CH_3	+	HCOOH	→	CH_4	+	COOH	3.33×10^{-44}	3.86×10^{-32}
OH	+	HCOOH	→	H_2O	+	COOH	1.70×10^{-47}	2.21×10^{-34}
CH_3O	+	HCOOH	→	CH_3OH	+	COOH	3.10×10^{-63}	2.12×10^{-45}
CH_2OH	+	HCOOH	→	CH_3OH	+	COOH	4.38×10^{-69}	1.69×10^{-46}
HCO	+	HCOOH	→	H_2CO	+	COOH	1.53×10^{-59}	8.33×10^{-44}
H	+	H_2CO	→	H_2	+	HCO	8.46×10^{-01}	$6.02\times10^{+00}$
NH_2	+	H_2CO	→	NH_3	+	HCO	1.13×10^{-38}	9.41×10^{-30}
CH_3	+	H_2CO	→	CH_4	+	HCO	1.10×10^{-41}	1.30×10^{-29}
OH	+	H_2CO	→	H_2O	+	HCO	1.24×10^{-44}	1.68×10^{-31}
CH_3O	+	H_2CO	→	CH_3OH	+	HCO	3.71×10^{-58}	3.63×10^{-40}
CH_2OH	+	H_2CO	→	CH_3OH	+	HCO	6.89×10^{-59}	1.72×10^{-40}
H	+	NH_2CHO	→	H_2	+	NH_2CO	7.25×10^{-01}	$5.15\times10^{+00}$
NH_2	+	NH_2CHO	→	NH_3	+	NH_2CO	3.04×10^{-41}	2.51×10^{-32}
CH_3	+	NH_2CHO	→	CH_4	+	NH_2CO	4.32×10^{-44}	5.00×10^{-32}
OH	+	NH_2CHO	→	H_2O	+	NH_2CO	2.29×10^{-47}	2.97×10^{-34}
CH_3O	+	NH_2CHO	→	CH_3OH	+	NH_2CO	5.33×10^{-63}	3.70×10^{-45}
CH_2OH	+	NH_2CHO	→	CH_3OH	+	NH_2CO	7.54×10^{-69}	3.39×10^{-46}
HCO	+	NH_2CHO	→	H_2CO	+	NH_2CO	2.55×10^{-59}	1.39×10^{-43}
H	+	H_3CCHO	→	H_2	+	CH_3CO	7.30×10^{-01}	$5.19\times10^{+00}$
NH_2	+	H_3CCHO	→	NH_3	+	CH_3CO	4.07×10^{-41}	3.36×10^{-32}
CH_3	+	H_3CCHO	→	CH_4	+	CH_3CO	5.66×10^{-44}	6.55×10^{-32}
OH	+	H_3CCHO	→	H_2O	+	CH_3CO	3.12×10^{-47}	4.05×10^{-34}
CH_3O	+	H_3CCHO	→	CH_3OH	+	CH_3CO	9.33×10^{-63}	6.37×10^{-45}
CH_2OH	+	H_3CCHO	→	CH_3OH	+	CH_3CO	1.32×10^{-68}	4.88×10^{-46}
HCO	+	H_3CCHO	→	H_2CO	+	CH_3CO	4.32×10^{-59}	2.35×10^{-43}
H	+	CH_3OCHO	→	H_2	+	CH_3OCO	7.30×10^{-01}	$5.19\times10^{+00}$
NH_2	+	CH_3OCHO	→	NH_3	+	CH_3OCO	9.99×10^{-43}	8.24×10^{-34}
CH_3	+	CH_3OCHO	→	CH_4	+	CH_3OCO	1.80×10^{-45}	2.09×10^{-33}
OH	+	CH_3OCHO	→	H_2O	+	CH_3OCO	5.92×10^{-49}	7.67×10^{-36}
CH_3O	+	CH_3OCHO	→	CH_3OH	+	CH_3OCO	5.80×10^{-66}	3.95×10^{-48}
CH_2OH	+	CH_3OCHO	→	CH_3OH	+	CH_3OCO	8.20×10^{-72}	2.94×10^{-49}
HCO	+	CH_3OCHO	→	H_2CO	+	CH_3OCO	4.23×10^{-62}	2.30×10^{-46}
H	+	$HOCH_2CHO$	→	H_2	+	$HOCH_2CO$	6.73×10^{-01}	$4.78\times10^{+00}$
NH_2	+	$HOCH_2CHO$	→	NH_3	+	$HOCH_2CO$	1.20×10^{-42}	9.91×10^{-34}
CH_3	+	$HOCH_2CHO$	→	CH_4	+	$HOCH_2CO$	2.14×10^{-45}	2.48×10^{-33}
OH	+	$HOCH_2CHO$	→	H_2O	+	$HOCH_2CO$	7.21×10^{-49}	9.34×10^{-36}
CH_3O	+	$HOCH_2CHO$	→	CH_3OH	+	$HOCH_2CO$	8.46×10^{-66}	5.76×10^{-48}
CH_2OH	+	$HOCH_2CHO$	→	CH_3OH	+	$HOCH_2CO$	1.20×10^{-71}	4.28×10^{-49}
HCO	+	$HOCH_2CHO$	→	H_2CO	+	$HOCH_2CO$	6.02×10^{-62}	3.27×10^{-46}

Table 8.5: Aldehyde radical recombination reactions.

					k (cm^3/s)	
					10 K	50 K
H	+	NH_2CO	→	NH_2CHO	$1.92\times10^{+12}$	$1.36\times10^{+13}$
NH_2	+	NH_2CO	→	NH_2CONH_2	$3.12\times10^{+02}$	$2.58\times10^{+11}$
CH_3	+	NH_2CO	→	NH_2COCH_3	4.36×10^{-02}	$5.08\times10^{+10}$
OH	+	NH_2CO	→	NH_2COOH	2.09×10^{-03}	$2.74\times10^{+10}$
CH_3O	+	NH_2CO	→	NH_2COOCH_3	2.27×10^{-09}	$1.85\times10^{+09}$
CH_2OH	+	NH_2CO	→	NH_2COCH_2OH	1.08×10^{-12}	$4.22\times10^{+08}$
HCO	+	NH_2CO	→	NH_2COCHO	9.23×10^{-07}	$5.33\times10^{+09}$
H	+	CH_3CO	→	CH_3CHO	$1.92\times10^{+12}$	$1.36\times10^{+13}$
NH_2	+	CH_3CO	→	CH_3CONH_2	$3.12\times10^{+02}$	$2.58\times10^{+11}$
CH_3	+	CH_3CO	→	CH_3COCH_3	4.36×10^{-02}	$5.06\times10^{+10}$
OH	+	CH_3CO	→	CH_3COOH	2.09×10^{-03}	$2.71\times10^{+10}$
CH_3O	+	CH_3CO	→	CH_3COOCH_3	2.27×10^{-09}	$1.57\times10^{+09}$
CH_2OH	+	CH_3CO	→	CH_3COCH_2OH	3.21×10^{-15}	$1.45\times10^{+08}$
HCO	+	CH_3CO	→	CH_3COCHO	9.23×10^{-07}	$5.05\times10^{+09}$
H	+	CH_3OCO	→	CH_3OCHO	$1.92\times10^{+12}$	$1.36\times10^{+13}$
NH_2	+	CH_3OCO	→	CH_3OCONH_2	$3.12\times10^{+02}$	$2.58\times10^{+11}$
CH_3	+	CH_3OCO	→	CH_3OCOCH_3	4.36×10^{-02}	$5.05\times10^{+10}$
OH	+	CH_3OCO	→	CH_3OCOOH	2.09×10^{-03}	$2.71\times10^{+10}$
CH_3O	+	CH_3OCO	→	$CH_3OCOOCH_3$	2.27×10^{-09}	$1.54\times10^{+09}$
CH_2OH	+	CH_3OCO	→	CH_3OCOCH_2OH	3.20×10^{-15}	$1.15\times10^{+08}$
HCO	+	CH_3OCO	→	$CH_3OCOCHO$	9.23×10^{-07}	$5.02\times10^{+09}$
H	+	$HOCH_2CO$	→	$HOCH_2CHO$	$1.92\times10^{+12}$	$1.36\times10^{+13}$
NH_2	+	$HOCH_2CO$	→	$HOCH_2CONH_2$	$3.12\times10^{+02}$	$2.58\times10^{+11}$
CH_3	+	$HOCH_2CO$	→	$HOCH_2COCH_3$	4.36×10^{-02}	$5.05\times10^{+10}$
OH	+	$HOCH_2CO$	→	$HOCH_2COOH$	2.09×10^{-03}	$2.71\times10^{+10}$
CH_3O	+	$HOCH_2CO$	→	$HOCH_2COOCH_3$	2.27×10^{-09}	$1.54\times10^{+09}$
CH_2OH	+	$HOCH_2CO$	→	$HOCH_2COCH_2OH$	3.20×10^{-15}	$1.15\times10^{+08}$
HCO	+	$HOCH_2CO$	→	$HOCH_2COCHO$	9.23×10^{-07}	$5.02\times10^{+09}$
H	+	COOH	→	HCOOH	$1.92\times10^{+12}$	$1.36\times10^{+13}$
NH_2	+	COOH	→	NH_2COOH	$3.12\times10^{+02}$	$2.58\times10^{+11}$
CH_3	+	COOH	→	CH_3COOH	4.36×10^{-02}	$5.08\times10^{+10}$
OH	+	COOH	→	HOCOOH	2.09×10^{-03}	$2.73\times10^{+10}$
CH_3O	+	COOH	→	CH_3OCOOH	2.27×10^{-09}	$1.77\times10^{+09}$
CH_2OH	+	COOH	→	$HOCH_2COOH$	2.41×10^{-13}	$3.42\times10^{+08}$
HCO	+	COOH	→	OHCCOOH	9.23×10^{-07}	$5.25\times10^{+09}$

8.3.2 Determination of the Rate Constants

The rate constants for these reactions were derived in the manner outlined in reference [69] and depend on the diffusion rates, R_{diff}, of the two species involved. R_{diff} is the inverse of the diffusion time, t_{diff}, which is equal to the product of the hopping time, t_{hop}, and the density of surface sites on the grain, N_s ($\sim 10^6$). The hopping time can be determined by the relationship

$$t_{hop} = \nu_0^{-1} e^{E_b/kT} \tag{8.1}$$

where ν_0 is the characteristic vibrational frequency for the adsorbed species, E_b is the potential energy barrier between adjacent surface potential energy wells, k is the Boltzmann constant, and T is the temperature of the grain. E_b is approximated as $0.3E_D$, the barrier to diffusion, and ν_0 is also related to this quantity by the equation:

$$\nu_0 = (2n_s E_D/\pi^2 m)^{1/2} \tag{8.2}$$

where m is the mass of the species, and n_s is the surface density of sites ($\sim 1.5\times 10^{15}$ cm^{-2}). R_{diff} can therefore be determined by the relationship:

$$R_{diff} = \frac{(2n_s E_D/\pi^2 m)^{1/2} e^{-0.3E_D/kT}}{N_s} \tag{8.3}$$

The rate coefficient for the reaction between two species, k_{ij}, can be determined by the relationship:

$$k_{ij} = \kappa_{ij} \frac{R_{diff,i} + R_{diff,j}}{n_d} \tag{8.4}$$

where n_d is the number density of grains ($\sim 2.66 \times 10^{-7}$ cm^{-3}) and κ_{ij} is the probability for the reaction to occur. This probability is unity for a reaction with no activation barrier, such as radical-radical combination reactions. For a reaction with activation energy E_a, κ_{ij} is expressed as:

$$\kappa_{ij} = e^{-2a/\hbar(2\mu E_a)^{1/2}} \tag{8.5}$$

which is the exponential portion of the probability for quantum mechanical tunneling through a barrier of thickness a (1 Å).

Higher temperatures may be required to initiate more complex reactions on the grain surface since the heavier radicals will become more mobile at these temperatures. The diffusion barriers from references [12] and [69] were used to determine the diffusion rates at 10 and 50 K for the photolysis radicals as well as aldehyde radicals, and these values are presented in Table 8.6. All aldehyde proton abstraction barriers are estimated to be 5030 K (10 kcal/mol), which is the upper threshold for the barriers determined in the *ab initio* studies [77].

The reaction rates at 10 and 50 K were calculated from this information and are presented in Tables 8.2–8.5.

8.3.3 Discussion

The diffusion rates shown in Table 8.6 indicate that the simpler photolysis products will dominate grain surface chemistry at low temperatures. H will clearly be the most mobile species on grain surfaces, and so it is likely to immediately react with any radical produced during photolysis at 10 K. This mechanism indicates a buildup of simple species such as CH_3OH, H_2O, CH_4, NH_3, and H_2CO on cold grain surfaces, a conclusion

Table 8.6: Diffusion barriers and rates for reactive surface species.

	E_D (kcal/mol)	E_D (K)	R_{diff} (s^{-1}) 10 K	50 K
H	0.7	350	$5.100\times10^{+04}$	$3.62\times10^{+05}$
C	1.6	800	4.855×10^{-05}	$1.07\times10^{+04}$
O	1.6	800	4.207×10^{-05}	$9.24\times10^{+03}$
CH	1.3	654	3.377×10^{-03}	$2.22\times10^{+04}$
CH_2	1.9	956	4.581×10^{-07}	$4.23\times10^{+03}$
CO	2.4	1207	1.920×10^{-10}	$7.44\times10^{+02}$
OH	2.5	1258	5.557×10^{-11}	$7.20\times10^{+02}$
HCO	3.0	1509	2.456×10^{-14}	$1.34\times10^{+02}$
NH_2	1.7	855	8.302×10^{-06}	$6.85\times10^{+03}$
CH_3	2.3	1157	1.161×10^{-09}	$1.34\times10^{+03}$
CH_3O	3.4	1710	6.030×10^{-17}	$4.11\times10^{+01}$
CH_2OH	4.3	2163	8.523×10^{-23}	$3.05\times10^{+00}$
COOH	4.0	2012	6.324×10^{-21}	$6.04\times10^{+00}$
HCOOH	5.1	2565	4.335×10^{-28}	2.44×10^{-01}
H_2CO	3.5	1761	1.375×10^{-17}	$3.13\times10^{+01}$
NH_2CO	3.9	1962	2.857×10^{-20}	$8.16\times10^{+00}$
CH_3CO	4.7	2364	1.804×10^{-25}	8.10×10^{-01}
CH_3OCO	6.2	3119	2.590×10^{-35}	8.57×10^{-03}
$HOCH_2CO$	6.9	3471	7.032×10^{-40}	1.09×10^{-03}
NH_2CHO	4.7	2364	1.764×10^{-25}	7.91×10^{-01}
CH_3CHO	5.4	2716	4.920×10^{-30}	1.04×10^{-01}
CH_3OCHO	6.5	3270	2.838×10^{-37}	3.52×10^{-03}
$HOCH_2CHO$	7.4	3722	3.838×10^{-43}	2.50×10^{-04}

Note: Quantum tunneling dominates over diffusion for H at 10 K, and so the H tunneling rate is given at this temperature.

reinforced by recent observational studies of interstellar ices, which have abundance ratios of H_2O:CO_2:H_2CO:CO:CH_3OH:NH_3 of 100:18:12:10:8:7 [83].

At 50 K, however, the diffusion rates of the other radicals increase significantly, and so more complex species could form in this type of environment if the diffusion rates are comparable to the arrival rate of H from the gas phase. The hydrogen accretion rate from the gas phase can be calculated by the following equation:

$$dn_{H,grain}/dt = \pi r^2 (2kT/m)^{1/2} n_{H,gas} m \zeta n_g \tag{8.6}$$

The gas phase hydrogen density, $n_{H,gas}$, can be approximated as 2×10^{-4} $n_{T,gas}$, and $n_{T,gas}$ is on the order of $\sim 10^4$ cm^{-3}. A sticking coefficient, ζ, of unity, an average grain radius, r, of 1×10^{-7} m, and a grain density, n_g, of 10^{-12} $n_{T,gas}$ can also be assumed. The flux of H from the gas phase is therefore on the order of 2×10^{-7} s^{-1} at both 10 and 50 K. The 50 K diffusion rates in Table 8.6 of the more complex radicals are indeed higher than this arrival rate, and so complex chemistry involving these species is certainly possible. Indeed, recent observations of UV-processed interstellar ices with the *Spitzer Space Telescope* reveal that HCOOH is enhanced in such regions [84].

The photolysis products presented in Table 8.1 are clearly important in the formation of compounds such as methyl formate and glycolaldehyde as well as all of the 3C compounds, and so their reactions should certainly be included in grain surface models. The 2C structural isomers methyl formate, acetic acid, and glycolaldehyde could indeed form in significant quantities from these processes. Direct comparisons can be made for these simpler species formed from radical-radical combinations using the information derived above and the observed interstellar ratios for the starting material. An analysis of the relative reaction rates of the HCO + radical combination reactions results in the abundance ratios shown in Table 8.7. The branching ratios discussed above were combined with a CH_3 production pathway branching ratio of 0.1 for the purposes of this calculation. The assumption was made here that the available H on the grain surface would be determined by its production from photolysis processes. H will be in steady flux between the grain surface and gas phase, and so this number is an underestimate of the total amount of H on the grain surface. This estimation, however, provides an upper limit for the amount of more complex species that could form in such environments.

This comparison shows that the calculated reaction rate coefficients may in fact be

Table 8.7: Observed and calculated abundance ratios for the products of HCO+radical combination reactions relative to formaldehyde at 50 K. The observed column densities are those determined for Sgr B2(N-LMH).

		$N_T/N_{T,formaldehyde}$	
Formula	Species	Observed	Predicted at 50 K
H_2CO	formaldehyde	1	1
NH_2CHO	formamide	6	1.6×10^{-03}
CH_3CHO	acetaldehyde	21	8.8×10^{-06}
HCOOH	formic acid	0.3	2.3×10^{-03}
CH_3OCHO	methyl formate	4	8.9×10^{-06}
$HOCH_2CHO$	glycolaldehyde	0.1	3.3×10^{-07}

underestimated if the abundance ratios in hot cores are truly linked to grain surface mechanisms. It is likely, however, that the simpler, more reactive species such as formic acid and glycolaldehyde may undergo more complex reactions either on the grain or in the gas phase in the hot core, and so these observed abundances may not truly reflect grain surface composition. Regardless, abstraction pathways are clearly competitive on grain surfaces in warm regions, and these types of reactions should be integrated into current astrochemical models.

It is also likely that the 3C species discussed in this thesis could be formed on grains if abstraction reactions can compete with radical-radical combination reactions and single-atom addition reactions. It is clear from the rates presented in Table 8.4 that hydrogen will dominate both formation and abstraction reactions at both temperatures, so formaldehyde will likely be the dominant product of such channels at 10 K. As is demonstrated by the analysis presented in Table 8.7, however, the other radical reaction channels with HCO are also possible at 50 K, and so other complex aldehydes will likely be present in warmer regions.

The *ab initio* studies of radical-aldehyde interactions indicate that hydrogen abstraction

reactions have much lower barriers than do addition reactions involving the carbonyl group [77]. The hydrogen abstraction routes alone are therefore enough to compete with the single-atom addition reactions considered in other models. Once the aldehyde radicals are formed, these species could recombine with any of the mobile radicals. The products of recombination with hydrogen will be the primary products of these reactions, but the more complex pathways involving heavier radicals are also possible at 50 K. Species such as dihydroxyacetone, dimethyl carbonate, and methyl glycolate may well form from such mechanisms, and an analysis similar to that conducted for the simpler species in Table 8.7 can be used to investigate the predicted relative ratios of these isomers. Such an analysis reveals that the relative ratios of these species should be roughly 1:8300:8000, respectively. These results follow the trend reflected by the observational results, and once again demonstrate the need for aldehyde proton abstraction reactions to be incorporated into grain surface models.

It is clear from these preliminary analyses that grain surface chemistry has the potential to achieve considerable complexity. H addition reactions dominate the grain surface chemistry at low temperature, forming simple species such as water, methanol, and formaldehyde. Photolysis of simple grain mantle constituents leads to the production of surface radicals that can efficiently compete with H addition reactions at warmer temperatures, and so periodic thermal processing of grain mantles will lead to the buildup of more complex species such as formic acid, methyl formate, formamide, acetaldehyde, and glycolaldehyde. Aldehyde proton abstraction reactions can efficiently compete with single-atom addition reactions at both low and high temperatures, and so the mobile radicals can then react with the resultant aldehyde radicals to form more complex species such as those investigated in this thesis. Simpler species will be favored at low temperature, but

these radicals may also be stored in the grain mantle at low temperature and undergo more complex reactions upon grain mantle heating in hot core regions.

8.4 Future Work

The chemical network presented above indicates that complex molecule formation on grains should be reincorporated into interstellar chemistry models. Additional observational studies are required to investigate these revised chemical models once predictions for other complex species are obtained. Definitive observational tests of grain surface chemistry are quite limited, however. Observational searches for complex molecules in interstellar ices are difficult because individual spectral features are unresolvable. In addition, accretion disk regions with high gas phase abundances of complex species are smaller than the spatial resolution of current observatories. This limitation will be overcome upon the commissioning of the Combined Array for Millimeter Astronomy (CARMA) and Atacama Large Millimeter Array (ALMA) observatories over the next several years.

In the meantime, more sensitive studies of hot core sources combined with the direct study of grain mantle species in regions of grain mantle disruption are required. The first investigations of hot corinos, where the dynamical timescales are short and gas phase material remains primarily unprocessed, show a similar level of molecular complexity to high mass hot cores (see references [75] and [2]). Likewise, investigation of shocked regions in the Galactic Center also indicates large column densities of grain mantle material (see reference [18]).

Deep, broadband surveys of the Orion Compact Ridge and Sgr B2(N-LMH) sources are underway with a new 4 GHz IF bandwidth 1.3 mm SIS receiver at the CSO, and such studies should provide the spectral information necessary to identify previously undetected

complex species. A double sideband spectrum of the Orion Compact Ridge, the first result of this survey, is shown in Figure 8.2. It must be stressed that this spectrum is preliminary, as it has not been fully temperature or frequency calibrated. An RMS level on the order of 20 mK was reached with these observations, however, and the spectral line density at this sensitivity level is clearly quite high.

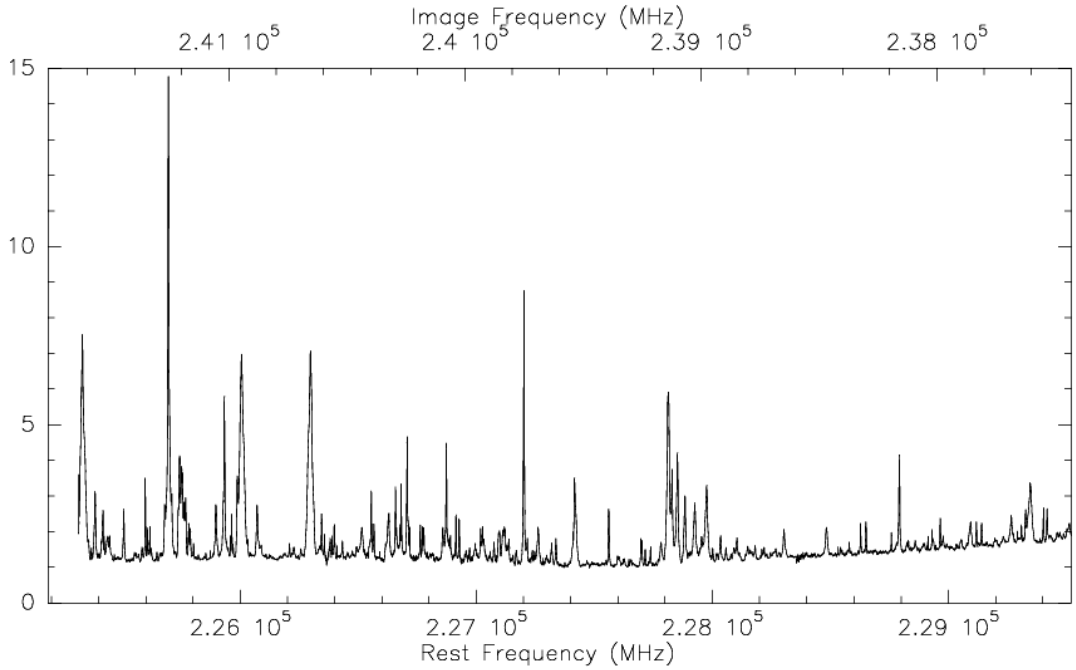

Figure 8.2: Initial results from a deep broadband line survey of the Orion Compact Ridge. The temperature and frequency calibrations are preliminary, but the RMS level is ∼20 mK.

Similar, if not more complicated, spectra are expected from the CASIMIR instrument on SOFIA and the HIFI instrument on the Herschel Observatory. Laboratory investigations to support these observations are also extremely important, and so experiments such as those detailed in this work should be continued for other complex molecules of interest. The laboratory spectral information available in the frequency ranges of these instruments is also quite limited, and so further THz studies are required to support these observations.